Inorganic Chemistry

Article

pubs.acs.org/IC

Peculiar Behavior of (U,Am)$O_{2-\delta}$ Compounds for High Americium Contents Evidenced by XRD, XAS, and Raman Spectroscopy

Florent Lebreton,[†] Denis Horlait,[†] Richard Caraballo,[‡] Philippe M. Martin,[§] Andreas C. Scheinost,[∥] Andre Rossberg,[∥] Christophe Jégou,[‡] and Thibaud Delahaye*[,†]

[†]CEA, DEN, DTEC/SDTC/LEMA, F-30207 Bagnols-sur-Cèze Cedex, France

[‡]CEA, DEN, DTCD/SECM/LMPA, F-30207 Bagnols-sur-Cèze Cedex, France

[§]CEA, DEN, DEC/SESC/LLCC, F-13108 Saint-Paul-lez-Durance Cedex, France

[∥]Helmholtz Zentrum Dresden Rossendorf, Institute of Resource Ecology, P.O. Box 10119, 01314 Dresden, Germany

ABSTRACT: In $U_{1-x}Am_xO_{2\pm\delta}$ compounds with low americium content ($x \leq 20$ atom %) and oxygen-to-metal (O/M) ratios close to 2.0, Am^{III+} cations are charge-balanced by an equivalent amount of U^{V+} cations while the fluorite structure of pure $U^{IV+}O_2$ is maintained. Up to now, it is unknown whether this observation also holds for higher americium contents. In this study, we combined X-ray diffraction with Raman and X-ray absorption spectroscopies to investigate a $U_{0.5}Am_{0.5}O_{2\pm\delta}$ compound. Our results indicate that americium is again only present as Am^{III+}, while U^{V+} remains below the amount required for charge balance. Unlike lower americium contents, this leads to an overall oxygen hypostoichiometry with an average O/M ratio of 1.92(2). The cationic sublattice is only slightly affected by the coexistence of large amounts of reduced (Am^{III+}) and oxidized (U^{V+}) cations, whereas significant deviations from the fluorite structure are evidenced by both extended X-ray absorption fine structure and Raman spectroscopies in the oxygen sublattice, with the observation of both vacancies and interstitials, the latter being apparently consistent with the insertion of U_6O_{12} cuboctahedral-type clusters (as observed in the U_4O_9 or U_3O_7 phases). These results thus highlight the specificities of uranium−americium mixed oxides, which behave more like trivalent lanthanide-doped UO_2 than $U_{1-x}Pu_xO_{2\pm\delta}$ MOX fuels.

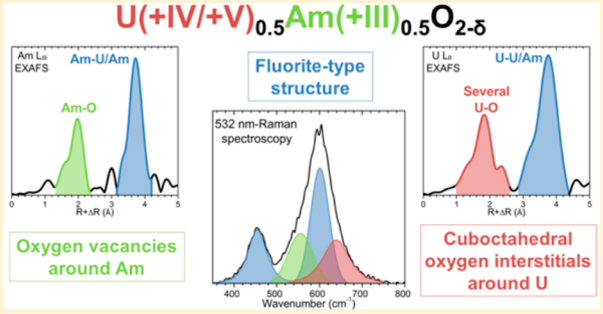

INTRODUCTION

Single and mixed dioxides of actinide (and of some lanthanide) elements stable in the IV+ oxidation state are known to crystallize under a fluorite-type structure [space group $Fm\bar{3}m$ (No. 225)], which can be described as a face-centered-cubic sublattice of cations (actinides or lanthanides) in which the oxygen anions occupy the tetragonal sites or as a simple cubic sublattice of oxygen in which half of the cubic sites are occupied by a cation. Most of these elements are, however, also stable under lower (M^{III+}) or higher (M^{V+} and M^{VI+}) oxidation states, which leads to mixed cationic oxidation states in the structure, compensated for by variations of the oxygen content, often designated as the oxygen-to-metal (O/M) ratio. From a structural point of view, these O/M variations can lead to structural transitions from the fluorite structure, which is the case for some end members of these systems (such as Pu_2O_3, Am_2O_3, and UO_3), but the fluorite $Fm\bar{3}m$ structure remains generally stable over wide ranges of O/M ratios, especially at high temperature, as low as 1.66 and as high as 2.24 in the case of the U−O system for instance.[1] This wide range is made possible by the ability of the fluorite structure to accommodate oxygen vacancies under oxygen hypostoichiometry (in the case of mixed III+/IV+ oxidation states) and interstitials under oxygen hyperstoichiometry (for mixed IV+/V+, or even VI+, oxidation states). In the case of oxygen hypostoichiometry, the structural consequence of O/M ratio variation is the formation of vacancies in the oxygen sublattice, generally without significant modifications of the cationic one.[2] In the case of oxygen hyperstoichiometry, for uranium oxides, for example, the main distortions of the fluorite structure occur in the oxygen sublattice, with only minor modifications of the cationic one. Willis, for example, proposed the formation of 2:2:2 clusters caused by the displacement of oxygen anions in the ⟨110⟩ and ⟨111⟩ directions, for O/M ratios under 2.25.[3,4] Such compounds thus correspond to the $UO_{2+\delta}$ domain, which is present at high temperatures on the U−O phase diagram.[1,5] At lower temperatures, oxygen hyperstoichiometry leads to the formation of U_4O_9 and metastable U_3O_7 compounds through the insertion of four interstitial oxygen anions in some of the oxygen cubes and a slight displacement of surrounding cations to form U_6O_{12} cuboctahedra.[6−11] The latter are responsible for additional U−O (close to 2.2 and 2.6 Å) and U−U distances, as

Received: June 17, 2015
Published: September 25, 2015

DOI: 10.1021/acs.inorgchem.5b01357
Inorg. Chem. 2015, 54, 9749−9760

well as the presence of uranium cations surrounded by 9 or 10 oxygen anions.

Concerning mixed actinide oxides, previous studies have shown that reduced III+ and oxidized V+/VI+ cations do not typically coexist. In $U_{1-x}Pu_xO_{2\pm\delta}$ compounds, for instance, Pu^{IV+} and U^{IV+} cations coexist with Pu^{III+} cations in the case of oxygen hypostoichiometry but with U^{V+} in the case of hyperstoichiometry.[1] The structure of such compounds can thus be approximatively described based on those respectively reported for $PuO_{2-\delta}$ and $UO_{2+\varepsilon}$ domains. Recent studies showed, however, that the case of $U_{1-x}Am_xO_{2\pm\delta}$ compounds (currently investigated for potential use as americium-bearing transmutation targets for nuclear waste long-term radiotoxicity attenuation)[12−15] was different. Despite the similarities between plutonium and americium oxides (both exist for O/M ratios ranging from 1.5 to 2 with similar phase diagrams in the corresponding domains)[16] and thus the stability of americium as both Am^{III+} and Am^{IV+}, several studies showed that Am^{III+} and U^{V+} cations coexist in single-phase $U_{1-x}Am_xO_{2\pm\delta}$ compounds.[17−22] Using X-ray absorption near-edge spectroscopy (XANES), Prieur et al. found that $U_{1-x}Am_xO_{2\pm\delta}$ compounds with Am/(U + Am) ratios comprised of between 10 and 20 atom % were composed of U^{IV+}, U^{V+}, and Am^{III+} (but no Am^{IV+}) cations with equivalent U^{V+} and Am^{III+} contents, leading to O/M ratios of 2.00(1).[17] Additional studies performed by X-ray diffraction (XRD) and extended X-ray absorption fine structure (EXAFS) showed that this charge distribution occurs without significant structural modifications.[17,23] Only the direct consequences of the difference in the ionic radii between the cations (Am^{III+}, 1.09 Å; U^{IV+}, 1.00 Å; U^{V+}, about 0.9 Å in 8-fold coordination)[24] were observed: shortening of the average U−O distances and lengthening of the average Am−O distances, as well as a slight increase of the structural disorder [namely, the Debye−Waller factor from X-ray absorption spectroscopy (XAS) and microstrain from XRD] with the Am/(U + Am) ratio.[17,18,20,23]

In the aforementioned XAS reports, the considered Am contents remained relatively low [Am/(U + Am) ≤ 20 atom %], and U^{IV+} was always found to be the main cation present, which might help to explain the preservation of the fluorite structure and, more precisely, of its oxygen sublattice. Regarding higher americium contents, some papers report the synthesis of $U_{1-x}Am_xO_{2\pm\delta}$ solid solutions with x values up to 0.5.[23,25,26] Using X-ray photoelectron spectroscopy (XPS) to study a $U_{0.5}Am_{0.5}O_{2-\delta}$ sample, Mayer et al. reported that americium was only present as Am^{III+}, whereas uranium's overall oxidation state is above IV+.[27] Suzuki et al. applied density functional theory (DFT) to a stoichiometric $U_{0.5}Am_{0.5}O_2$ compound and calculated that the americium and uranium oxidation states would respectively be III+ and V+.[28] If these studies give a first insight into the charge distribution in $U_{0.5}Am_{0.5}O_{2\pm\delta}$ compounds, no information related to its structural consequences is discussed. In this study, we therefore focused on the effect of a high Am/(U + Am) ratio (50 atom %) on the local structure of a $U_{1-x}Am_xO_{2\pm\delta}$ compound via XRD, XAS (XANES/EXAFS), and Raman spectroscopy. This report thereby provides the first recorded Raman spectra of uranium−americium mixed oxides.

EXPERIMENTAL SECTION

Synthesis. Synthesis of the $U_{0.5}Am_{0.5}O_{2\pm\delta}$ (and $U_{0.85}Am_{0.15}O_{2\pm\delta}$) samples used for this study was previously described in detail.[26] In a few words, the samples were prepared from single $UO_{2+\delta}$ and $AmO_{2-\delta}$ precursor powders using the UMACS process.[15] This process allows for the fabrication of dense and homogeneous pellets, even from single oxide precursors (UO_2 and AmO_2), by avoiding reactive sintering and the chemical and microstructural heterogeneities sometimes reported for such a process.[29−31] The two powders are first mixed by ball milling, pelletized, and heat-treated at 2023 K for 8 h under flowing $Ar/H_2/O_2$ for an oxygen potential of −420 kJ·mol^{-1}. The sample is then crushed by ball milling, and the obtained powder is used for the formation of a new green pellet, which is sintered at 2023 K for 4 h under flowing Ar/H_2 for an oxygen potential of −570 kJ·mol^{-1}. After synthesis, an Am/(U + Am) ratio of 49(1) atom % was estimated by thermal ionization mass spectrometry. A UO_2 reference sample was also prepared from the same $UO_{2+\delta}$ powder batch and sintered with the test samples.

XRD. XRD was performed using a Bruker D8 Advance diffractometer in $\theta-\theta$ Bragg−Brentano geometry, especially modified for radioactive material measurements. It is equipped with a copper source [$\lambda(K\alpha_1/\alpha_2)$ = 1.540598/1.54443 Å] and a Bruker LYNXEYE linear detector with a 3° opening angle. Diffractograms were recorded from 2θ = 25 to 120°, with a 2θ = 0.01° step and a counting time of 1.1 s·step^{-1} for a total recording duration of about 3 h. For peak position correction, Au powder was added as a 2θ standard. Analysis and refinement of the X-ray diffractograms were performed using the *Fullprof Suite* software[32] by applying the Le Bail method[33] and a Thompson−Cox−Hastings function for peak profile description,[34] as previously reported.[23]

XAS. XAS measurements were performed at the European Synchrotron Radiation Facility (ESRF; Grenoble, France) on the Rossendorf Beamline (BM20) with a current of 170−200 mA in the storage ring (at 6.0 GeV). The XAS sample was a transmission pellet prepared from of a mixture of powdered $U_{0.5}Am_{0.5}O_{2\pm\delta}$ and boron nitride (which is invisible to X-ray). The obtained pellet was double-sealed in a contamination-free Teflon/polyethylene sample holder.

Spectra were collected at the U L_{III}, Am L_{III}, and U L_{II} edges at 17166, 18510, and 20948 eV, respectively, in both transmission and fluorescence modes, using Oxford ionization chambers and a Canberra energy-dispersive 13-element germanium solid-state detector with a digital amplifier (XIA-XMAP). The beam size and distance between the sample and detector were adapted to remain in the linear range of the fluorescence detector. A double Si(111) crystal monochromator was used for energy selection, and the calibration was performed using metallic foils whose K edges are close to the edges of interest, i.e., yttrium (17038 eV), zirconium (17998 eV), and molybdenum (20000 eV). XANES spectra were recorded at the U and Am L_{III} edges, while Am L_{III} and U L_{II} were used for EXAFS measurements (up to k = 18 and 13.5 Å^{-1}, respectively). U L_{II} is preferred over U L_{III} because neptunium present in the samples (produced by α decay of ^{241}Am) would limit the EXAFS spectra at U L_{III} at k = 10.5 Å^{-1}. The temperature of the samples was maintained at approximately 20 K during the measurements using a closed-cycle helium cryostat. The contribution of thermal vibrations to σ^2 (Debye−Waller factor determined by EXAFS spectrum refinement) can thus be considered negligible, so σ^2 mainly represents the (static) structural disorder. The UO_2 sample was also used as a reference compound for the fluorite structure for EXAFS measurements. Its structure was checked by XRD, which indicates the presence of a sole fluorite structure and a lattice parameter of 5.4708(5) Å, close to that expected for an O/M ratio of 2.00 [5.47127(8) Å].[35]

Data analyses and refinements were performed using *Athena* and *Artemis* software[36,37] and *FEFF 8.40* for ab initio calculations of EXAFS spectra. XANES spectra were normalized using a linear function for pre- and postedge approximation. The first zero crossings of the first and second derivatives were used to determine the white line (WL) and inflection point (E_0) positions, respectively. The average oxidation states of the cations were determined by linear combinations of reference spectra to fit experimental normalized absorption spectra of the sample considered. The reference compounds used were $U^{IV+}O_{2.00(1)}$, $(U^{IV+}_{1/2}U^{V+}_{1/2})_4O_9$,[10] and $(U^{V+}_{2/3}U^{VI+}_{1/3})_3O_8$,[38] as well as two mixed U/Am^{III+} compounds [an oxide, $U_{0.85}Am_{0.15}O_{2.00(1)}$,[17] and an oxalate, $(U^{IV+}_{0.9}Am^{III+}_{0.1})_2(C_2O_4)_5{\cdot}6H_2O$[39−41]] and $Am^{IV+}O_2$,

DOI: 10.1021/acs.inorgchem.5b01357
Inorg. Chem. 2015, 54, 9749−9760

whose XANES spectra were previously recorded at the same beamline. Fourier transforms of the EXAFS spectra were extracted using a Hanning window between 3.5 and 11 $Å^{-1}$ and between 3.5 and 14 $Å^{-1}$ for the U L_{II} and Am L_{III} edges, respectively, in both cases with a *dk* factor of 2.

Two structural models were used for ab initio EXAFS calculations. The first one corresponds to a standard fluorite structure in which each cation is surrounded by 8 oxygen anions at $a \times \sqrt{3}/4$, 12 cations at $a \times \sqrt{2}/2$, 24 oxygen anions at $a \times \sqrt{11}/4$, and 6 cations at *a*. In this case, the four corresponding two-legged paths were included to fit the spectra, as well as two three-legged and two four-legged multiple scattering paths, based on their relatively high magnitudes. The three-legged paths are Abs−O2−U/Am1−Abs (Abs representing the absorbing atom) and Abs−O1−O2−Abs. The four-legged ones are both Abs−O1−Abs−O1−Abs, with angles of 0° (the linear one) or 180° (that for which the first and second oxygen atoms are the same). The second structural model used is based on the fluorite cluster in which one of the oxygen atoms in the first shell is replaced by two interstitial oxygen atoms located in interstitial sites corresponding to those reported by Garrido et al. for the cuboctahedral oxygen cluster described for U_3O_7.[7] In this case, only five two-legged paths were included for the fit, corresponding to the two first oxygen atoms in normal fluorite positions, the two first oxygen atoms in cuboctahedral positions, and the first cation. Fits were performed between 1.4 and 4.5 Å and between 1.6 and 6 Å respectively at the U L_{II} and Am L_{III} edges, with a *k* weight of 3. The shift in the threshold energy (ΔE_0) was varied as a global parameter.

Raman Spectroscopy. Raman spectroscopy characterizations were performed in a hot cell, using a Horiba Jobin-Yvon LabRam HR800 Raman spectrometer coupled to an optical microscope developed by Optique Peter (Lyon, France) including a six-objective turret from which $a \times 100$ was used. The laser employed is a frequency-doubled YAG (λ = 532 nm) with an output power of 200 mW, which can be adjusted by a variable filter installed at its output. A 600 lines·mm^{-1} network was used, giving a spectral resolution of 1.7 cm^{-1}. Further details regarding the apparatus were given in previous papers.[42−45] Presented spectra were typically collected by the accumulation of 10 spectra with an acquisition time of 30 s. Determined band positions correspond to the average of 10 different spectra, i.e., 10 different locations on the sample. Uncertainties given in brackets correspond to the dispersion of the band positions in the 10 spectra.

Because only a few Raman spectra of $U_{1-x}Am_xO_{2\pm\delta}$ have been reported in the literature (Naji et al. recently reported the spectra for x = 0.1 and 0.2),[46] a 15 atom % Am sample, previously characterized by XRD and XAS,[17] was also analyzed by Raman spectroscopy (after annealing). The samples used for the measurements were two sintered pellets, of the respective compositions $U_{0.85}Am_{0.15}O_{2.00(1)}$[17] and $U_{0.5}Am_{0.5}O_{1.93(2)}$ (details regarding the O/M ratio of this sample are given in further sections). Because the initial aim was to determine Raman spectra of an undamaged $U_{0.5}Am_{0.5}O_{2\pm\delta}$ structure, the pellet was heated under Ar/H_2 for 1 h at 1373 K under an oxygen potential of −550 kJ·mol^{-1} to ensure radio-induced defect recovery,[47] and Raman spectroscopy measurements were performed 1, 4, and 14 days after annealing. It has to be noted that such a heat treatment could not be performed for the XAS samples because they needed to be prepared in advance. Because during optical microscopy observation the two faces of the pellet appeared to be contaminated by dust, presumably because of contact with different surfaces during their preparation, handling, and storage, measurements were instead performed on the edge of the pellet.

For each sample, no significant differences between all acquired spectra were found (not only in active modes and their positions but also in band relative intensities). Notably, no evolutions of the Raman spectra with time were observed for the time considered. In a previous XRD monitoring experiment, in which similar samples were also annealed under a reducing atmosphere and stored under the same conditions as those for this study, a partial and progressive oxidation of the samples during the first weeks following annealing was reported.[23] The most probable explanation for this discrepancy is that the analysis depth of Raman spectroscopy (several tens of nanometers) is lower than that of XRD (several micrometers). Thus, if oxidation of the extreme surface of the sample is complete after less than 24 h, the progression of oxidation cannot be evidenced by Raman spectroscopy and, correlatively, the spectra obtained are relative to $U_{0.85}Am_{0.15}O_{2\pm\delta}$ and $U_{0.5}Am_{0.5}O_{2\pm\delta}$ already oxidized under their storage conditions.

Deconvolution of the spectra in several bands was performed using the Horiba *LabSpec* software in the 350−750 and 350−800 cm^{-1} domains respectively for the 15 and 50 atom % Am samples. Prior to this operation, each spectrum was smoothed and its background contribution was subtracted. Lorentzian or pseudo-Voigt functions were used to simulate the bands. Bands were approximately positioned before the fit, but their positions were not fixed during it.

RESULTS

XRD. The X-ray diffractogram of $U_{0.5}Am_{0.5}O_{2\pm\delta}$ recorded after a storage period very close to that of the XAS sample (aged for 160 days) is given in Figure 1. Only peaks

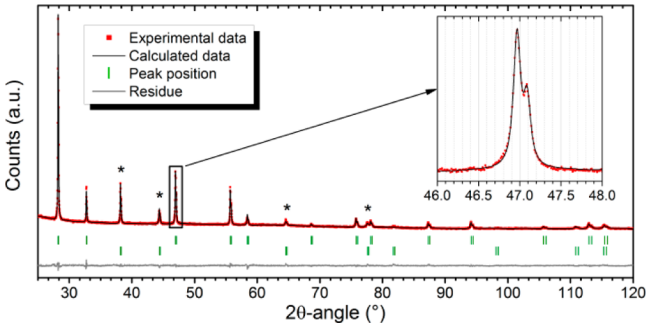

Figure 1. X-ray diffractogram of the $U_{0.5}Am_{0.5}O_{2\pm\delta}$ sample 160 days after sintering (asterisks point out peaks corresponding to Au used as a reference for 2θ positions).

corresponding to a single fluorite structure were identified, as evidenced in previous studies of similar samples.[23,26] A lattice parameter of 5.4670(5) Å was determined by refinement. The latter, however, includes a contribution of self-irradiation effects, which induce lattice expansion over the first months of storage because of the α activity of the ^{241}Am isotope (1.3×10^{11} Bq·g^{-1}).[23,48−50] An undamaged lattice parameter of 5.454(1) Å was determined from the 160-day value and by using $U_{0.5}Am_{0.5}O_{2\pm\delta}$ radio-induced structural swelling data reported in the literature.[23]

XAS. *XANES.* The $U_{0.5}Am_{0.5}O_{2\pm\delta}$ XANES Am L_{III} spectrum (Figure 2) is well aligned with that of the Am^{III+} reference. The determined WL positions of these two spectra are also close [18517.7(5) eV], whereas that of the Am^{IV+} reference is about 4 eV higher [18521.6(5) eV]. Americium thus seems to be present almost exclusively as Am^{III+} in the sample, which is confirmed by linear combination fitting of the sample spectrum with reference compound spectra (presented in Figure 4), with the best fit for 100% of the Am^{III+} reference spectrum, without any contributions from AmO_2.

At the U L_{III} edge (Figure 3), the WL position [17177.9(5) eV] is between those of the hyperstoichiometric reference compounds U_4O_9 [17176.7(5) eV] and U_3O_8 [17179.6(5) eV]. The overall uranium oxidation state thereby lies between 4.5 (U_4O_9) and 5.33 (U_3O_8). The sample WL shape is similar to that of U_4O_9 and thus clearly differs from that of UO_2 (or even U_3O_8), which is mostly caused by distortion of the cubic symmetry and the resulting additional U−O distances (cf. the Introduction) in U_4O_9. The XANES spectrum of the sample,

DOI: 10.1021/acs.inorgchem.5b01357
Inorg. Chem. 2015, 54, 9749−9760

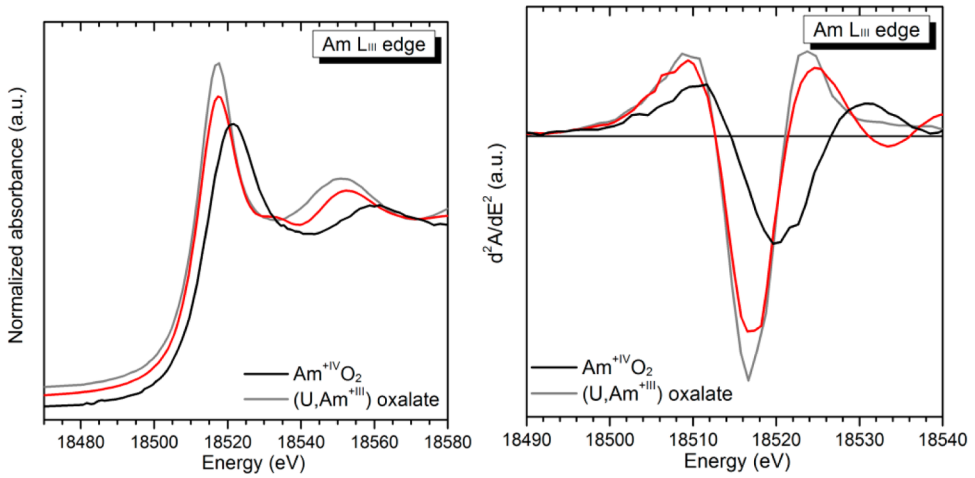

Figure 2. XANES spectrum at the Am L_{III} edge (left) and its second derivative (right) of the $U_{0.5}Am_{0.5}O_{2\pm\delta}$ sample (in red) compared to those of AmO_2 and $(U_{0.9}Am_{0.1})$ oxalate.

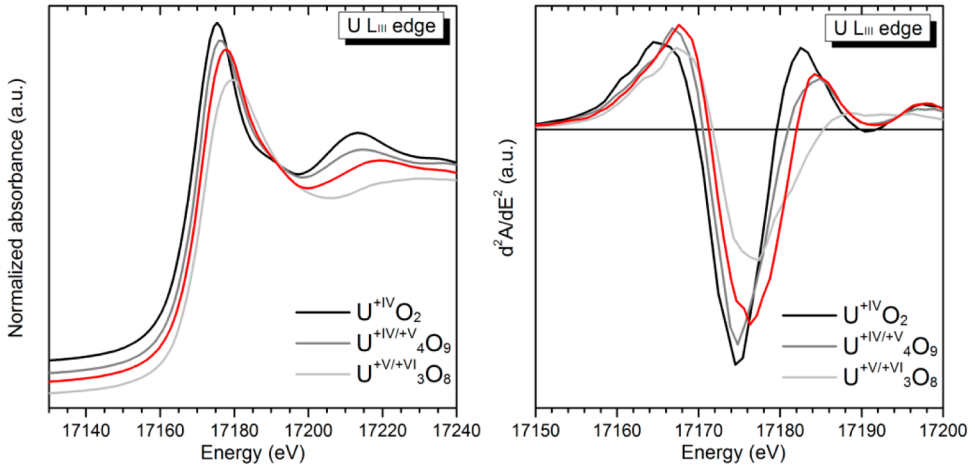

Figure 3. XANES spectra at the U L_{III} edge (left) and its second derivative (right) of the $U_{0.5}Am_{0.5}O_{2\pm\delta}$ sample (in red) compared to those of UO_2, U_4O_9, and U_3O_8.

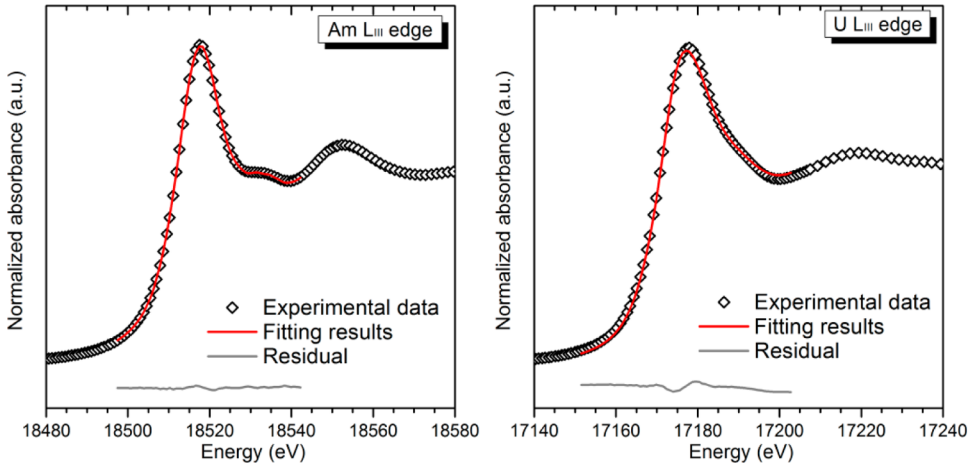

Figure 4. Fit of the XANES spectra of the $U_{0.5}Am_{0.5}O_{2\pm\delta}$ sample by the linear combination of reference compounds at the Am L_{III} (left) and U L_{III} (right) edges.

consequently, indicates the presence of such distortions in the oxygen sublattice. Fitting the sample spectrum with linear combinations of U_4O_9 and U_3O_8, an average oxidation state of 4.65(3) is obtained [the best fits being obtained for 82(4)% U_4O_9 and 18(4)% U_3O_8]. The residual of the fit is, however, higher than that observed at the Am L_{III} edge because of a lower disorder in the cationic sublattice in comparison to that in U_4O_9 (as is notably pointed out by the X-ray diffractogram in

DOI: 10.1021/acs.inorgchem.5b01357
Inorg. Chem. 2015, 54, 9749−9760

Figure 1). On the basis of the oxidation state determined by the linear combination fitting of the XANES spectrum, the O/(U + Am) ratio of the sample can be estimated at 1.92(2), indicating an overall oxygen hypostoichiometry of the sample.

EXAFS. The Am L_{III} edge EXAFS spectrum is presented in Figure 5, together with its Fourier transform. This spectrum

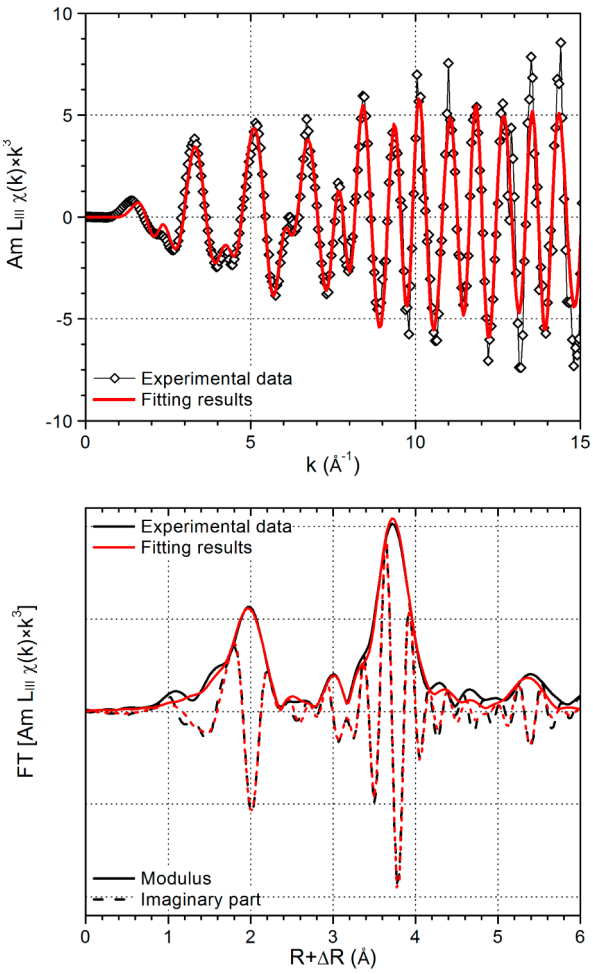

Figure 5. Experimental k^3-weighted Am L_{III} edge EXAFS spectrum (upper graph) and its Fourier transform (lower graph) of the $U_{0.5}Am_{0.5}O_{1.92(2)}$ compound (black) and respective shell fit (red).

corresponds to what is expected in the case of a fluorite structure, with two main contributions, and is thus consistent with the XRD results pointing out the presence of a single fluorite structure. The first peak at about 1.9 Å corresponds to the contribution of the first oxygen shell, and the second peak, at about 3.8 Å, is mainly due to the first cation shell. The fit was consequently performed using the fluorite model described in the Experimental Section. The results of the fit are presented in Figure 5 and the obtained parameters given in Table 1. The presence of a fluorite local structure around americium cations is confirmed by the reasonable agreement between experimental and fitted spectra, as illustrated by the *R*-factor value of 0.013. Moreover, the coordination number for the cationic shells is close to the value expected for a nondefective fluorite structure.

The main difference from a defect-free fluorite structure is the low coordination number obtained for the first oxygen shell [about 6.8(5) instead of 8]. This result seems to indicate the presence of oxygen vacancies surrounding americium cations, with about 15(6)% of vacancies. No significant deviation from the expected value is observed for the second oxidation shell [22(5) compared to 24], even though a deviation would most likely be hindered by the larger uncertainty. Regarding interatomic distances, Am−cation distances are close to those calculated from XRD. The first Am−O distance is longer than expected from XRD, which is notably a consequence of the relatively large ionic radius of the Am^{III+} cation compared to the other identified cations. Debye−Waller factors are higher than those determined for a UO_2 compound, in line with the presence of vacancies inducing local distortions (i.e., a broadening of the first U−O distance distribution) in the oxygen sublattice, notably around americium cations.

The sample spectrum at the U L_{II} edge appears to be different from that of a fluorite local structure, as evidenced in the comparison of k^1-weighted spectra of the sample and several uranium oxide references (UO_2, U_4O_9, and U_3O_8) presented in Figure 6. Compared to a UO_2 reference compound, the sample spectrum shows a discrepancy in the *k* region of 3−7 $Å^{-1}$, in which the main contribution is that of the first oxygen shell. Its Fourier transform remains composed of two main peaks, but their intensity is lower than that for UO_2, especially for the peak around 1.9 Å, which is also significantly broader and seems to include additional contributions at longer and shorter distances. This spectrum thus resembles that of the U_4O_9 compound, particularly the contribution of the first oxygen shells ($R < 2.5$ Å). The fit was thus performed using the second model presented in the Experimental Section, for which some of the oxygen fluorite positions are replaced by cuboctahedral positions, leading to two additional U−O bonds.

The fitted results are shown along with the experimental data in Figure 7, and the obtained fit parameters are given in Table 1. A reasonable graphical agreement is observed between the experimental and fitted data, further confirmed by a relatively low *R* factor. The two additional U−O distances corresponding to the cuboctahedral positions are determined to be 2.28(1) and 2.87(1) Å, in contrast to the oxygen distance in the fluorite position of 2.31(1) Å, i.e., lower than expected from XRD. On the basis of the obtained coordination numbers, oxygen anions remain mostly present in the normal fluorite positions. The coordination numbers of the first cationic and second anionic shells, i.e., the unmodified shells, are consistent with a defect-free fluorite structure, and their interatomic distances are close to those expected from the XRD results. The Debye−Waller factors of these two shells are also larger than those obtained for the americium local environment, which can be attributed to the disorder increase induced by the presence of additional oxygen positions, particularly for $U-O_{fluo.}1$.

Raman Spectroscopy. The best spectra acquired for $U_{0.85}Am_{0.15}O_{2.00(1)}$ and $U_{0.5}Am_{0.5}O_{1.92(2)}$ (those with the best noise/signal ratio) are presented in Figure 8. Some Raman spectra were acquired up to 4000 cm^{-1}, but bands were only observed up to ∼1250 and ∼700 cm^{-1}, respectively, for the 15 and 50 atom % Am samples. For $U_{0.85}Am_{0.15}O_{2.00(1)}$, a narrow band (denoted as C in Figure 8) is observed around 446(1) cm^{-1}, as well as a broad one, denoted as D, around 551(3) cm^{-1}, which includes a shoulder at 630−640 cm^{-1}, denoted as E, and another one at 1148(3) cm^{-1}, denoted as F. Some of the latter bands were also noted in $U_{0.5}Am_{0.5}O_{1.92(2)}$ spectra, notably C [at 457(2) cm^{-1}], D [a broad band centered at 602(5) cm^{-1}], and E [present around 530(10) cm^{-1} as a

DOI: 10.1021/acs.inorgchem.5b01357
Inorg. Chem. 2015, 54, 9749−9760

Table 1. Structural Parameters Obtained by Refinement of $U_{0.5}Am_{0.5}O_{2-\delta}$ EXAFS Spectra Presented in Figures 5 and 7

sample edge	sphere	distance (Å) XRD	distance (Å) EXAFS	coordination number	Debye–Waller factor σ^2 (Å^2)	correlation factor R
UO_2 (reference), U L_{III}	O1	2.369(1)	2.355(5)	7.9(5)	0.0031(5)	0.008 (domain: 1.6–6 Å)
	U1	3.868(1)	3.866(5)	11.9(5)	0.0015(5)	
	O2	4.536(1)	4.52(1)	26(5)	0.005(2)	
	U2	5.471(1)	5.46(2)	6(1)	0.003(1)	
50% Am (sample), Am L_{III}	O1	2.367(1)	2.422(5)	6.8(5)	0.0065(5)	0.017 (domain: 1.6–6 Å)
	Am/U1	3.866(1)	3.852(5)	11.6(5)	0.0047(5)	
	O2	4.533(1)	4.43(2)	22(5)	0.010(2)	
	Am/U2	5.467(1)	5.46(2)	6(1)	0.005(1)	
50% Am (sample), U L_{II}	$O_{cubo.}1$[a]		2.28(1)	1.2 (5)	0.003[b]	0.013 (domain: 1.41–4.5 Å)
	$O_{fluo.}1$[a]	2.367(1)	2.31(1)	5.9(5)	0.018(3)	
	$O_{cubo.}2$[a]		2.87(1)	1.2(5)	0.003[b]	
	Am/U1	3.866(1)	3.86(1)	12.0(5)	0.0053(5)	
	$O_{fluo.}2$[a]	4.533(1)	4.52(2)	28(5)	0.014(5)	

[a]Oxygen atoms noted O and $O_{fluo.}$ are those in normal positions (8c Wyckoff sites) for a fluorite structure, whereas those noted $O_{cubo.}$ are those in sites corresponding to the cuboctahedral clusters (48i Wyckoff sites), as described by Garrido et al.[7] [b]Debye–Waller factors for oxygen in cuboctahedral positions are fixed during the fit.

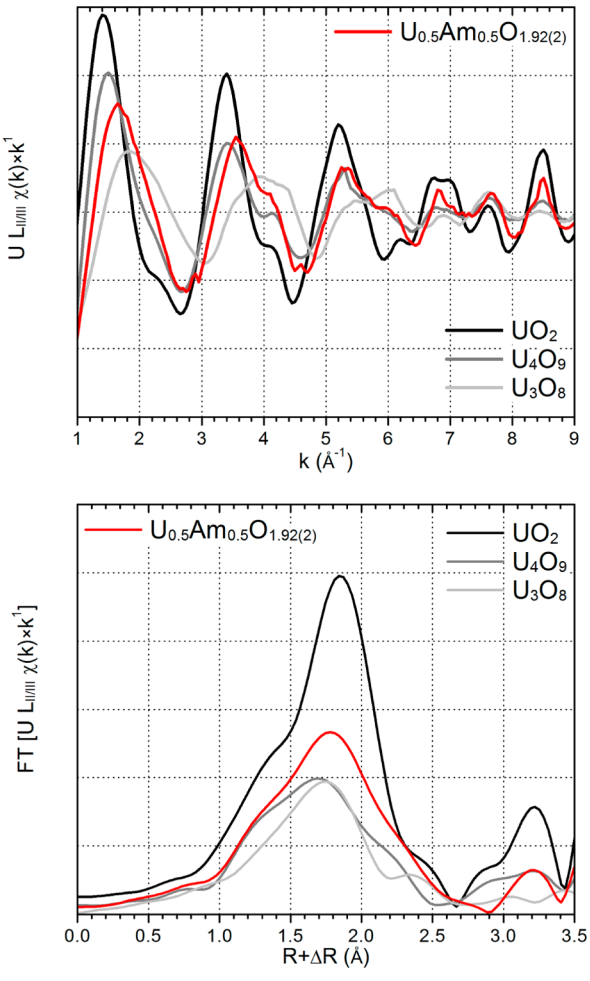

Figure 6. k^1-weighted EXAFS spectrum (upper graph) and its Fourier transform (lower graph) of the $U_{0.5}Am_{0.5}O_{1.92(2)}$ compound at the U L_{II} edge compared to those of uranium oxide reference samples (a k^1 weight is applied here to highlight the influence of the first oxygen shell).

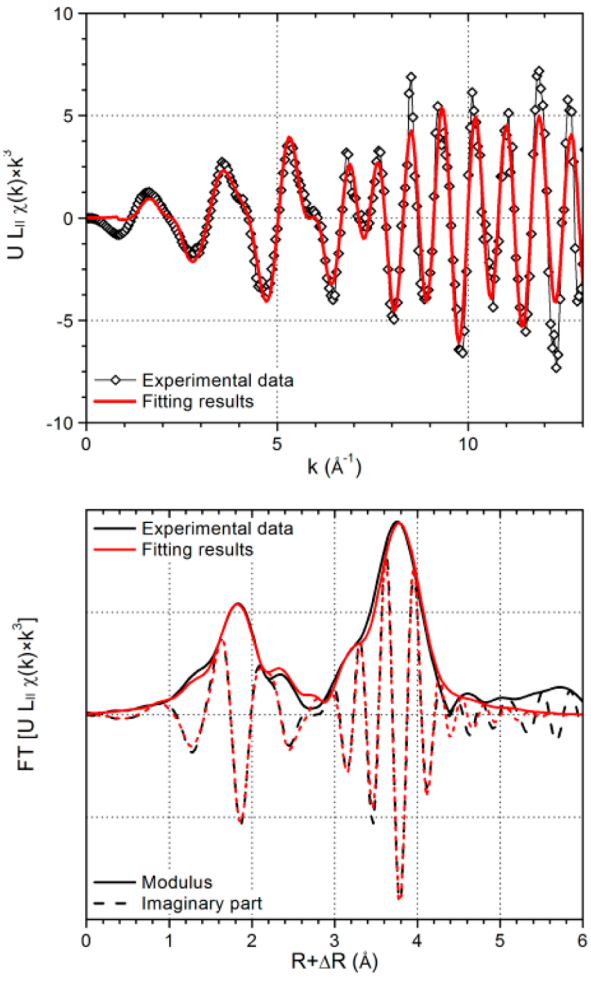

Figure 7. Experimental k^3-weighted U L_{II} edge EXAFS spectrum (upper graph) and its Fourier transform (lower graph) for the $U_{0.5}Am_{0.5}O_{1.92(2)}$ compound (black) and respective shell fit (red).

shoulder of D]. Two small bands, denoted as A and B, might also be present in the spectra respectively around 140 and 320 cm^{-1}, but no bands were observed around 1150 cm^{-1}. Deconvolution in several bands was performed in the 350–800 cm^{-1} range and is presented in Figure 9. The positions of the different peaks, determined by visual observation or by deconvolution (when applicable), are summarized in Table 2.

DOI: 10.1021/acs.inorgchem.5b01357
Inorg. Chem. 2015, 54, 9749–9760

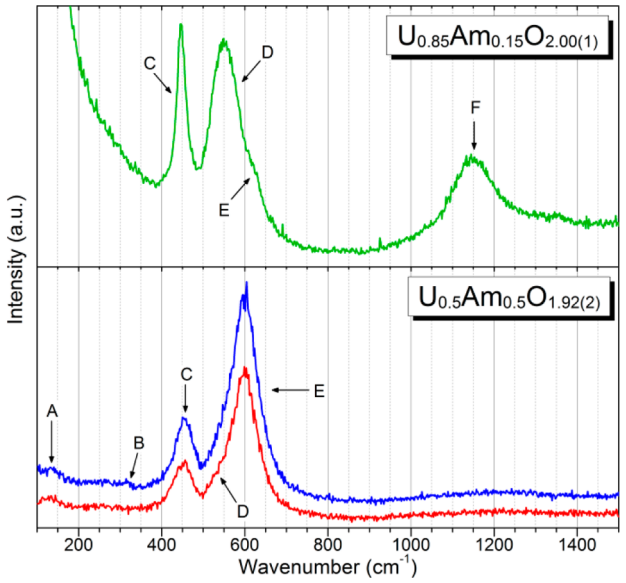

Figure 8. Raman spectra collected for (upper graph) the $U_{0.85}Am_{0.15}O_{2.00(1)}$ and (lower graph) the $U_{0.50}Am_{0.50}O_{1.92(2)}$ samples. Letters indicate the peaks identified.

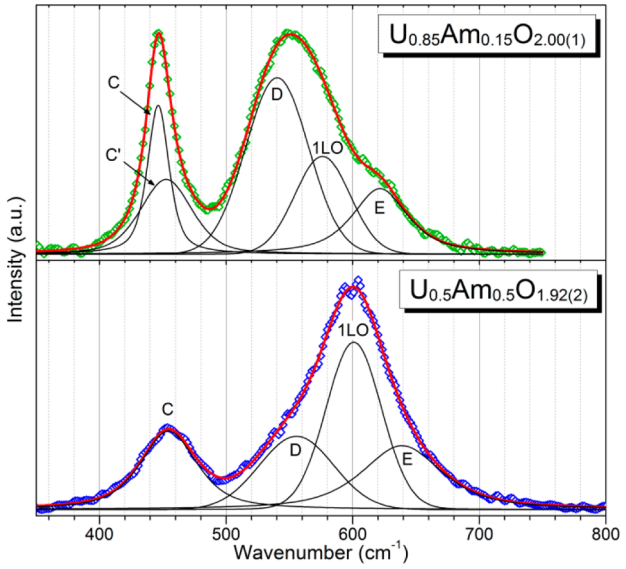

Figure 9. Results of the Raman spectrum deconvolution in the 350–800 cm^{-1} domain for (upper graph) the $U_{0.85}Am_{0.15}O_{2.00(1)}$ and (lower graph) the $U_{0.50}Am_{0.50}O_{1.92(2)}$ samples. Colored dots are the smoothed experimental data and the lines the fitted results (the red line being the sum of the different contributions represented as black lines).

In the case of the $U_{0.5}Am_{0.5}O_{1.92(2)}$ sample, deconvolution was applied to the two spectra presented in Figure 8 and gave similar results. The average position of each band is thus reported in Table 2.

T_{2g} and Related Bands. In MO_2 compounds with a defect-free fluorite structure, group theory[51] and published data[51−53] predict only one Raman active mode (T_{2g}), which corresponds to the vibration of the M−O bond with the cation M surrounded by eight oxygen anions in a cubic environment. The vibration of this band is usually minimally affected by M nature, and as a consequence, this mode could be expected for wavenumbers close to that reported for stoichiometric UO_2 (445 cm^{-1}),[53−57] as was the case in the study of Naji et al., who

Table 2. Band Positions and Their Respective Assignments for the Two $U_{1-x}Am_xO_{2\pm\delta}$ Samples Compared to the Positions Reported in the Literature for $UO_{2+\delta}$ and $U_{1-x}M^{III+}{}_xO_{2-\delta}$ Compounds

	experimental position (cm^{-1})		literature data		
band	$U_{0.85}Am_{0.15}O_{2.00(1)}$	$U_{0.5}Am_{0.5}O_{1.92(2)}$	compound	position (cm^{-1})	ref
B_{1g}?		140(5)[a]	$UO_{2+\delta}$	155	57
B_{1g}?		320(5)[a]	$UO_{2+\delta}$	315	57
T_{2g}	446(1)	453(3)	UO_2	445	53−57
"U_4O_9"	453(1)		U_4O_9	455	57, 59
$A_g + F_g$	540(1)	555(1)	(M^{IV+}, Ln^{III+}) $O_{2-\delta}$[b]	530 → 595	58, 60−64
1LO	576(1)	600(1)[c]	UO_2	575	42, 53−57, 65, 66
A_{1g}	621(1)	638(2)	$UO_{2+\delta}$	630	45, 57
2LO	1148(3)[a]		UO_2	1150	42, 53−57, 65, 66

[a]Positions determined visually (and not by deconvolution). [b]M = U, Th, Ce. [c]The assignment of a 1LO mode to the 600 cm^{-1} mode remains hypothetical based on available data.

reported T_{2g} close to 445 cm^{-1} for $U_{1-x}Am_xO_2$ samples with x = 0.1 and 02.[46] Thus, C modes observed around 450 cm^{-1} for both samples [respectively at 446(1) and 457(2) cm^{-1} for the 15 and 50 atom % Am compounds] should be T_{2g}.

Although the position of T_{2g} in UO_2 is precisely known (despite small variations between authors) to be about 445 cm^{-1}, that of AmO_2 has never been rigorously identified. We recently reported an AmO_2 Raman spectrum displaying a single band close to 390 cm^{-1} that might correspond to T_{2g} because of its high intensity, but this assignment remains doubtful.[44] As discussed by Naji et al.,[46] a position 50−100 cm^{-1} higher would have been expected based on the known T_{2g} positions of other actinide dioxides: ThO_2 (465 cm^{-1}),[52,54,58] UO_2 (445 cm^{-1}),[53−57] NpO_2 (465 cm^{-1}),[52−54] or PuO_2 (475 cm^{-1}).[42,53,54] T_{2g} of $U_{0.5}Am_{0.5}O_{1.92(2)}$ is blue-shifted by 8 cm^{-1} compared to UO_2[53−57] and, more surprisingly, by more than 60 cm^{-1} compared to the supposed T_{2g} of AmO_2,[44] i.e., both to higher wavenumbers, while an intermediate band position could have been expected. The uncertainties surrounding the true position of T_{2g} of AmO_2 preclude any further conclusions about the T_{2g} position of the samples. A red shift of T_{2g} with the americium content seems to be observed, which could be considered to be consistent with a position of the AmO_2 T_{2g} at a higher wavenumber than reported. Nonetheless, the XANES results showed that americium is only present as Am^{III+} and accommodated in a fluorite environment in both samples, so the Raman results for AmO_2 might not be suitable for comparison here. Am_2O_3 Raman data are also unfit for comparison because $Am_2O_{3+\delta}$ has stable crystalline structures, $Ia\bar{3}$ and $P\bar{3}m1$, which differ from that of $U_{1-x}Am_xO_{2\pm\delta}$ and $U_{0.5}Am_{0.5}O_{1.92(2)}$.[44,46,48,50] The presence of aliovalent cations could thus result in shifts compared to the usual T_{2g} position for UO_2, as observed in both samples.

For $U_{0.85}Am_{0.15}O_{2.00(1)}$, deconvolution reveals a second band denoted as C′ at 452(1) cm^{-1}, i.e., at a slightly higher wavenumber than the T_{2g} band. On the basis of previous studies, such a band is expected in hyperstoichiometric uranium oxides (notably in U_4O_9)[57,59] even though it was not always

DOI: 10.1021/acs.inorgchem.5b01357
Inorg. Chem. 2015, 54, 9749−9760

identified in these compounds, notably because of its proximity to T_{2g}. This band is accordingly difficult to differentiate from a higher wavenumber shift of the T_{2g} position, as is probably the case for the $U_{0.5}Am_{0.5}O_{1.92(2)}$ spectra (for which the T_{2g} position is about 10 cm^{-1} higher). As observed in both Figures 8 and 9, this band could be neither observed nor deconvoluted from T_{2g}. The presence of such a band would thus indicate similarities between the sample(s) and the U_4O_9 structure, which is discussed in more detail in a further section.

1LO and 2LO. In Raman spectra of some MO_2 compounds (UO_2, PuO_2, $U_{1-x}Pu_xO_2$, $U_{1-x}Ce_xO_2$, or $U_{1-x}Th_xO_2$), the normally forbidden mode 1LO (at 575 cm^{-1}) and its overtones, 2LO (1150 cm^{-1}), 3LO (1725 cm^{-1}), etc., can sometimes be observed.[42,46,53−57,65,66] Livneh and Sterer showed that the LO series is activated through a resonance process and is thus dependent on the laser energy and the sample's electronic properties, i.e., its band gap, because a laser energy slightly higher than the gap energy is required.[56] For instance, the spectrum of a UO_2 sample with a band gap close to 1.9 eV will present an intense 2LO band (even more intense than its T_{2g}) when studied with a 514 nm laser (2.41 eV), whereas 785 nm (1.58 eV) or 632.8 nm (1.96 eV) lasers produce significantly weaker 2LO bands (or even no band at all).[46,53,56,67] Further studies by different research groups also reported that the closer the O/M ratio to 2.00, the higher the relative intensity of the 2LO band compared to that of T_{2g} and that a significant deviation from the oxygen stoichiometry could lead to the extinction of the 2LO band.[53−57]

For $U_{0.85}Am_{0.15}O_{2.00(1)}$, band F [observed at 1148(3) cm^{-1}] presumably corresponds to the 2LO band, indicating that the laser used activates the LO series for this composition. The presence of the 2LO mode would also be consistent with the O/M ratio previously reported by XANES: 2.00(1).[17] This band is, however, not as intense as it can be for an as defect-free as possible UO_2 sample,[55,56] which might indicate a slight deviation from the oxygen stoichiometry and/or modifications of the sample band gap compared to UO_2, for instance, because of the presence of americium. On the basis of the presence of the 2LO, a band corresponding to the 1LO mode can also be expected around 575 cm^{-1} and would confirm the results obtained by deconvolution, which include a contribution centered at around 575 cm^{-1}, as presented in Figure 9.

The $U_{0.5}Am_{0.5}O_{1.92(2)}$ Raman spectra do not include any bands around 1150 cm^{-1}, hence no 2LO mode. Its absence could be explained by a deviation from the stoichiometry [which would be consistent with the 1.92(2) O/M ratio determined by XANES] and/or by significant modifications of the electronic properties of the sample compared to UO_2. On the basis of DFT calculations, Suzuki et al. concluded that the band gap of stoichiometric $U_{0.5}Am_{0.5}O_2$ was approximatively 1.5 eV, hence larger than that of AmO_2 (1.3 eV) but still smaller than that of UO_2 (1.9 eV).[28] The difference between the band gap of $U_{0.5}Am_{0.5}O_2$ and the laser energy (2.33 eV for the 532 nm laser) is thus larger than that in the case of UO_2, which could be responsible for a decrease in the 2LO intensity or even its extinction. The present sample is, nevertheless, characterized by a significantly lower O/M ratio (based on XANES) than the theoretical compound of Suzuki et al., as well as by a modified oxygen sublattice (based on EXAFS), which might both have modified its electronic properties and band gap. The current data available thus do not allow for a clear explanation of the missing 2LO band in the 532 nm Raman spectrum of $U_{0.5}Am_{0.5}O_{1.92(2)}$. As a consequence, even though the absence of the 2LO band suggests that no 1LO mode should be identified for this sample, the uncertainty surrounding the reasons for the absence of the 2LO band precludes exclusion of a hypothetical 1LO mode.

Bands Related to Modifications of the Oxygen Sublattice. For both samples, the deconvolution attempts suggest the presence of a triplet of bands. Even though the closeness of these bands makes it difficult to obtain a perfect disambiguation of the spectra, it is possible to propose an identification of these bands based on similar results previously reported for nonstoichiometric uranium-based oxide samples.[45,68]

The highest-wavenumber band composing the triplet [respectively identified at 621(1) and 638(2) cm^{-1} for the 15 and 50 atom % Am compounds] is probably a signature of U_4O_9-type cuboctahedral oxygen clusters as previously reported.[57,59,64] Indeed, in their Raman spectroscopy study of $UO_{2+\delta}$ (with δ varying between 0 and 0.33), He and Shoesmith demonstrated the presence of such clusters in $UO_{2+\delta}$ compounds with $\delta \geq 0.15$ through a main band close to 630 cm^{-1}, accompanied by two weak bands at 155 and 315 cm^{-1}.[57] They based their argument on the analogue tetragonal ZrO_2 system, assigning the 630 cm^{-1} intense band to an A_{1g} mode and two smaller bands that they observed at 155 and 315 cm^{-1} (both B_{1g} stretch). The latter two might correspond to the small bands that seem to emerge at around 140 and 320 cm^{-1} in the $U_{0.5}Am_{0.5}O_{1.92(2)}$ spectra (Figure 8). However, their low intensities do not allow for a clear conclusion. Concerning $U_{0.85}Am_{0.15}O_{2.00(1)}$, no peaks except the one at 622(1) cm^{-1} associated with cuboctahedral oxygen clusters were identified. The Raman spectra could, nevertheless, be in accordance with the existence of cuboctahedral oxygen clusters in both samples.

The lowest-wavenumber band [respectively identified at 540(1) and 555(1) cm^{-1} for the 15 and 50 atom % Am compounds] of the triplet can be attributed to the same mode for both samples. In similar systems, such as $U_{1-x}Ln^{III+}{}_xO_{2-\delta}$ in which Ln^{III+} is a trivalent lanthanide cation, a Raman band at a comparable position was attributed to a local phonon mode caused by vacancies in the oxygen sublattice.[63,64,69] On the basis of other works on $Ce^{IV+}{}_{1-x}Ln^{III+}{}_xO_{2-x/2}$ and $Th^{IV+}{}_{1-x}Ln^{III+}{}_xO_{2-x/2}$ solid solutions, this mode could further be assigned to the M−O bond vibration with M in a cubic MO_8 environment, with at least one of the oxygen anions being replaced by a vacancy.[58,60,62] The presence of vacancies in the fluorite oxygen sublattice of both compounds would thus be in agreement with the Raman spectrum deconvolution.

For $U_{0.85}Am_{0.15}O_{2.00(1)}$, all bands observed are thus identified because the middle band of the triplet was already attributed to the 1LO mode. The middle band of the $U_{0.5}Am_{0.5}O_{1.92(2)}$ triplet, on the other hand, remains unassigned based on the information available in this study. This band could correspond to the 1LO mode. The position observed [600(1) cm^{-1}] is indeed rather close to the expected position (around 575 cm^{-1}, based on UO_2 literature data[42,53−57,65,66] and the Raman spectrum of $U_{0.85}Am_{0.15}O_{2.00(1)}$ in Figure 9). Regardless, no bands that could possibly correspond to a 2LO mode were observed for this sample. On the basis of the position shift and the absence of a 2LO mode, which could have clarified the expected 1LO position, the ascription of the 600 cm^{-1} band to the 1LO mode remains hypothetical.

Guimbretière et al. recently reported that the bands corresponding to oxygen hypo- and hyperstoichiometries (respectively around 550 and 630 cm^{-1}) could be activated

DOI: 10.1021/acs.inorgchem.5b01357
Inorg. Chem. 2015, 54, 9749−9760

by ion-beam irradiation (He^{2+}) in a UO_2 sample presenting an overall O/M ratio of 2.00.[68] They assumed that the irradiation-induced damage generates structural defects corresponding to local oxygen hypo- or hyperstoichiometries, thus activating the corresponding Raman bands that they observed at 530 and 635 cm^{-1}, respectively. In $U_{1-x}Am_xO_{2\pm\delta}$ compounds, the high α activity of ^{241}Am (1.3×10^{11} $Bq{\cdot}g^{-1}$) is known to be responsible for structural damage such as a slight increase of the structural disorder with time.[18,20,23,47,70] In the present case, $U_{0.85}Am_{0.15}O_{2.00(1)}$ and $U_{0.5}Am_{0.5}O_{1.92(2)}$ were studied up to 15 days after annealing, which respectively corresponds to 0.005 and 0.017 dpa.[23] For such low accumulated doses, the contribution from self-irradiation damage is negligible in comparison to the dose required to activate the ∼550 and ∼630 cm^{-1} bands observed, especially considering their relatively high intensities in the Raman spectra of both samples.

DISCUSSION

O/M Ratio and Oxidation Process. On the basis of the XANES results, an overall O/M ratio of 1.92(2) is obtained for the 50 atom % Am sample, in agreement with the absence of the 2LO mode in its Raman spectra (suggesting a deviation from the oxygen stoichiometry) and with the lattice parameter obtained from XRD. The latter is, after correction for radio-induced lattice swelling, equal to 5.454(1) Å, i.e. lower than that expected based on the a_0 values of other $U_{1-x}Am_xO_{2\pm\delta}$ compounds ($0 \leq x \leq 0.4$) and assuming a monotonous variation of the lattice parameters of $U_{1-x}Am_xO_{2.00(1)}$ compounds with x.[17,19,23]

Concerning the cationic charge distribution, the XANES results indicate the presence of americium only in the Am^{III+} state, agreeing with the results obtained by XPS by Mayer et al. on a similar composition.[27] In contrast, uranium is present in a partially oxidized state, and this compound thus has the same type of cationic charge distribution as $U_{1-x}Am_xO_{2\pm\delta}$ samples with lower americium contents (x comprised of between 5 and 20 atom %)[17−20,29,71] as well as that calculated by DFT for $U_{0.5}Am_{0.5}O_2$ by Suzuki et al.[28] Because the linear combination of the XANES spectrum was performed with U^{IV+}/U^{V+} and U^{V+}/U^{VI+} reference compounds (respectively U_4O_9 and U_3O_8), the mole fractions of these three cations are not directly available from XANES, but some information can be obtained otherwise. First, the Suzuki et al. DFT calculations indicate that uranium is only present as U^{V+} in a stoichiometric $U_{0.5}Am_{0.5}O_2$ compound.[28] The observed cuboctahedral clusters are generally associated solely with U^{V+} cations, of which a large amount are required for these clusters to form.[10] Moreover, the presence of U^{VI+} is not favored by the fluorite-derived structure of hyperstoichiometric uranium oxides: in the U−O system, the appearance of U^{VI+}, for instance, results in the formation of a U_3O_8 phase.[11] U^{VI+} cation presence should also be detected by Raman spectroscopy and EXAFS through a broad band around 800−900 cm^{-1}[64,72] and additional short U−O distances (about 1.7−1.8 Å),[73,74] which is not the case here. The presence of a significant amount of U^{VI+} in the $U_{0.5}Am_{0.5}O_{1.92(2)}$ sample is thus doubtful, and U^{IV+} and U^{V+} can be considered the only uranium cations present. According to XANES, U^{IV+} and U^{V+} mole fractions among cations would thus respectively be 18(2) and 33(2) atom %.

The determined composition, $U_{0.5}Am_{0.5}O_{1.92(2)}$, consequently presents a lower O/M ratio than those reported for samples with lower Am/(U + Am) contents (from 10 to 20 atom %). In another study, Horlait et al. showed that, during storage under ambient conditions after heat treatment under reducing conditions, $U_{1-x}Am_xO_{2\pm\delta}$ samples with x ranging from 7.5 to 50 atom % undergo a significant oxidation during the first days.[23] The O/M ratio estimated several weeks after the synthesis is thus the result of two successive processes: reduction during heat treatment under a reducing atmosphere, followed by oxidation during storage. Considering the low oxygen potential applied during the heat treatment (about −570 kJ mol^{-1}),[26] cations are most likely reduced to a state close to U^{IV+}/Am^{III+}, as was, for example, observed for a uranium and americium oxide mixture by in situ XRD.[30,50] Because the various XANES studies (including the present one) showed that americium remained present in the Am^{III+} state even after the oxidation process under ambient conditions,[17−20] the latter occurs through oxidation of U^{IV+} cations to U^{V+}, simultaneously with an O/M ratio increase.

In the case of the lowest Am/(U + Am) ratios (i.e., from 10 to 20 atom %), oxidation appears to stop for an O/M ratio close to 2.00,[17] whereas it stopped at a lower O/M ratio for the present 50 atom % Am compound. Considering the oxidizing storage conditions (0.2 atm of O_2), it is probable that in both cases this state does not correspond to thermodynamic equilibrium. It can be noted that the average uranium oxidation state reached, 4.65(3), is close to the upper limit of the existence of a fluorite-derived compound for uranium single oxides, i.e., U_3O_7, in which uranium's average oxidation state is 4.67.[7,10,75] In these materials, higher oxidation states of uranium are only made possible by heating at a temperature above ∼500 K, also leading to the formation of U_3O_8, which presents a structure significantly different from the fluorite-type one.[76] Furthermore, doped UO_2 (and notably M^{III+}-doped UO_2) materials possess an improved resistance to the formation of such U_3O_8-type domains.[76−79] Therefore, the oxidation of uranium cations in the $U_{0.5}Am_{0.5}O_{2-\delta}$ sample most likely stopped because the fluorite structure is unable to withstand a higher uranium oxidation state without structural modifications in the cationic sublattice and because the storage temperature (close to 300 K) does not allow the formation of U_3O_8. Oxidation of the sample could, however, have occurred through the oxidation of Am^{III+} cations to Am^{IV+}, but the XANES results clearly indicate that Am^{III+} cations remain stable. Although this can be a result of metastability, americium thus truly behaves as an M^{III+} cation upon substitution for uranium in UO_2, at least for Am/(U + Am) ratios ranging from 5 to 50 atom %,[17,71] although $Am^{III+}{}_2O_3$ is neither thermodynamically nor kinetically stable in ambient conditions.[44] The identified upper limit of cationic oxidation states, i.e., ($U^{4.67+}$, Am^{3+}), apparently corresponds to a metastable state of these mixed oxides, which might even be applicable not only to $U_{1-x}Am_xO_{2\pm\delta}$ compounds with other x values but also more generally to other similar $M^{III+}UO_{2\pm\delta}$ materials.

Structural Modifications. Although the O/M ratio estimated by XANES indicates the overall oxygen hypostoichiometry of the sample, it cannot directly give information on the possible structural modifications induced, notably in the oxygen sublattice, which can, however, be proposed through a comparison of the XRD, EXAFS and Raman spectroscopy results previously presented.

The three methods are in agreement concerning the conservation of the cationic sublattice of a fluorite-type structure. The XRD diagram only contains peaks derived from such a structure, indicating that there are no modifications of the cationic sublattice. The EXAFS results also concur in the

DOI: 10.1021/acs.inorgchem.5b01357
Inorg. Chem. 2015, 54, 9749−9760

preservation of the cationic sublattice because only one first shell cation−cation distance is observed, in contrast to what is found for U_4O_9 or U_3O_7 compounds in which slight displacements of some cations occur, leading to several cation−cation distances. Moreover, the interatomic distances between cations and the coordination numbers obtained are also consistent with the presence of a fluorite structure, and Debye−Waller factors do not indicate a steep increase of structural disorder in the cationic sublattice, although they are slightly higher than those found in the UO_2 reference sample, or even in $U_{1-x}Am_xO_{2\pm\delta}$ compounds with lower americium contents.[17] The presence of the T_{2g} mode in the Raman spectra, which is characteristic of the MO_8 cubic clusters of the fluorite structure, indicates that at least some of the oxygen anions remain in an environment identical with the only one existing in a defect-free $M^{IV+}O_2$ fluorite-type structure.

Raman spectroscopy also suggests, through the 555(1) cm^{-1} band, the presence of oxygen vacancies in the $U_{0.5}Am_{0.5}O_{1.92(2)}$ fluorite structure. These vacancies are evidenced by EXAFS too, notably around americium cations, which is to be expected because americium is only found in a reduced state. Raman spectroscopy and EXAFS results could also be consistent with the presence of oxygen cuboctahedral clusters in $U_{0.5}Am_{0.5}O_{1.92(2)}$, similar to those found in the U_4O_9 and U_3O_7 compounds, even though the deviations observed in the cationic sublattice of these two compounds are not observed here.[6−11]

The quantitative information obtained on these structural defects through EXAFS and Raman spectroscopy remains, nonetheless, limited. Through EXAFS, the oxygen coordination numbers around americium and uranium are respectively 6.8(5) and 6.5(5), but the closeness of the three first U−O distances does not allow for a precise estimation of the ratio of cuboctahedral clusters and thus of possible oxygen vacancies around uranium cations. The comparison between Raman spectra obtained for the $U_{0.5}Am_{0.5}O_{1.92(2)}$ and $U_{0.85}Am_{0.15}O_{2.00(1)}$ samples can, however, give some information. The Raman spectrum of the 15 atom % Am sample surprisingly indicates the presence of oxygen vacancies and cuboctahedral clusters, which were not identified by EXAFS on similar samples in previous works.[17−20] This discrepancy is due to the high sensitivity of Raman spectroscopy to modifications of local symmetry induced by defects such as oxygen vacancies and cuboctahedral clusters in fluorite-type MO_2 compounds.[57,58,62,63] These structural defects would then be present in $U_{1-x}Am_xO_{2\pm\delta}$ compounds even for low Am/(U + Am) ratios (such as 15 atom %) but at a lower content, which would not be surprising because the vacancies and cuboctahedral clusters are respectively directly and indirectly caused by the presence of reduced Am^{III+} cations (and the partial oxidation of uranium to U^{V+}, for which they are responsible). The lower defect concentration in the 15 atom % Am sample would, however, preclude their detection via EXAFS, which has a higher detection limit, especially for defects related to light atoms such as oxygen. The failure of XRD to detect the oxygen vacancies and cuboctahedral clusters can be reasonably explained by its even more limited sensitivity to the oxygen sublattice.

The XRD diagram obtained for $U_{0.5}Am_{0.5}O_{1.92(2)}$ is thus mostly representative of the cationic sublattice. The retention of an apparent defect-free fluorite indicates that the modifications that might occur in the oxygen sublattice do not have an important impact on the cationic sublattice of the fluorite structure. This resilience is made possible by the capacity of this structure to accommodate various structural defects, notably related to its low atomic density and the fact that cations only occupy half of the cubic positions in the oxygen sublattice. A slight local distortion of the fluorite structure could be expected in the vicinity of the oxygen vacancies and cuboctahedral clusters. The presence of such defects would thus partially explain the microstrain increase with the americium content determined by XRD in the $U_{1-x}Am_xO_{2\pm\delta}$ series ($0 \leq x \leq 0.5$)[23] because the higher the Am^{III+} content (and, in correlation, uranium's average oxidation state), the greater the expected amount of oxygen vacancies and cuboctahedral clusters.

CONCLUSION

XRD, EXAFS, and Raman spectroscopy were combined to perform a structural characterization of a mixed uranium−americium oxide with an Am/(U + Am) ratio close to 50 atom %. The results obtained highlight the same peculiar charge distribution as that reported for lower americium contents, i.e., the presence of americium only as Am^{III+}, whereas uranium is partially oxidized to U^{IV+}/U^{V+}. For such a high americium content, the equivalent O/M ratio obtained is about 1.92(2) and is thus significantly hypostoichiometric despite storage of the sample under ambient, thus oxidizing, conditions.

From a structural point of view, no significant deviations of the cationic sublattice were evidenced either from XRD, EXAFS, or Raman spectroscopy because the three techniques agree on preservation of the fluorite-type $Fm\bar{3}m$ structure. The oxygen sublattice, however, presents deviations from the fluorite structure. In agreement with the low O/M ratio determined, vacancies were identified through EXAFS (mostly around reduced Am^{III+} cations) and deconvolution of the Raman spectra suggests that the bands observed could be related to oxygen vacancies. These characterization techniques also point out that oxygen interstitials are present around the uranium cations. The latter could be present in the form of cuboctahedral clusters of oxygen anions (similar to those found in the hyperstoichiometric uranium oxides U_4O_9 and U_3O_7), as suggested by the cation−oxygen distances determined by EXAFS and deconvolution of Raman bands, even though further work would be required for a nonambiguous attribution of Raman bands to structural defects in uranium-based oxides. The combination of the results obtained by these three techniques would suggest that the $U_{0.5}Am_{0.5}O_{1.92(2)}$ compound presents defects corresponding to both hypo- and hyperstoichiometric MO_2 fluorite materials.

AUTHOR INFORMATION

Corresponding Author

*E-mail: thibaud.delahaye@cea.fr.

Author Contributions

All authors have given approval to the final version of the manuscript.

Notes

The authors declare no competing financial interest.

ACKNOWLEDGMENTS

The authors acknowledge P. Coste and M. Bataille for sample fabrication and preparation for XAS experiments and M. Génisson for Raman spectroscopy measurements. D.H. and F.L. thank the CEA PACFA program for financial support

DOI: 10.1021/acs.inorgchem.5b01357
Inorg. Chem. 2015, 54, 9749−9760

through postdoctoral and Ph.D. funding. The authors also acknowledge the ESRF (Grenoble, France) for a provision of synchrotron radiation facilities at BM20 (Rossendorf Beamline) and the FP7 (European Community's Seventh Framework Programme) Talisman project for its support.

REFERENCES

(1) Guéneau, C.; Dupin, N.; Sundman, B.; Martial, C.; Dumas, J.-C.; Gossé, S.; Chatain, S.; Bruycker, F. D.; Manara, D.; Konings, R. J. M. *J. Nucl. Mater.* **2011**, *419*, 145−167.
(2) Allen, G. C.; Tempest, P. A. *Proc. R. Soc. London, Ser. A* **1986**, *406*, 325−344.
(3) Willis, B. T. M. *Nature* **1963**, *197*, 755−756.
(4) Willis, B. T. M. *Acta Crystallogr., Sect. A: Cryst. Phys., Diffr., Theor. Gen. Crystallogr.* **1978**, *34*, 88−90.
(5) Guéneau, C.; Baichi, M.; Labroche, D.; Chatillon, C.; Sundman, B. *J. Nucl. Mater.* **2002**, *304*, 161−175.
(6) Bevan, D. J. M.; Grey, I. E.; Willis, B. T. M. *J. Solid State Chem.* **1986**, *61*, 1−7.
(7) Garrido, F.; Ibberson, R. M.; Nowicki, L.; Willis, B. T. M. *J. Nucl. Mater.* **2003**, *322*, 87−89.
(8) Cooper, R. I.; Willis, B. T. M. *Acta Crystallogr., Sect. A: Found. Crystallogr.* **2004**, *60*, 322−325.
(9) Garrido, F.; Hannon, A. C.; Ibberson, R. M.; Nowicki, L.; Willis, B. T. M. *Inorg. Chem.* **2006**, *45*, 8408−8413.
(10) Desgranges, L.; Baldinozzi, G.; Siméone, D.; Fischer, H. E. *Inorg. Chem.* **2011**, *50*, 6146−6151.
(11) Andersson, D. A.; Baldinozzi, G.; Desgranges, L.; Conradson, D. R.; Conradson, S. D. *Inorg. Chem.* **2013**, *52*, 2769−2778.
(12) Bejaoui, S. *Proceedings of GLOBAL 2011*, Makuhari, Japan, 2011.
(13) D'Agata, E.; Hania, P. R.; Bejaoui, S.; Sciolla, C.; Wyatt, T.; Hannink, M. H. C.; Herlet, N.; Jankowiak, A.; Klaassen, F. C.; Bonnerot, J.-M. *Nucl. Eng. Des.* **2012**, *242*, 413−419.
(14) Lebreton, F.; Prieur, D.; Horlait, D.; Delahaye, T.; Jankowiak, A.; Léorier, C.; Jorion, F.; Gavilan, E.; Desmoulière, F. *J. Nucl. Mater.* **2013**, *438*, 99−107.
(15) Delahaye, T.; Lebreton, F.; Horlait, D.; Herlet, N.; Dehaudt, P. *J. Nucl. Mater.* **2013**, *432*, 305−312.
(16) Sari, C.; Zamorani, E. *J. Nucl. Mater.* **1970**, *37*, 324−330.
(17) Prieur, D.; Martin, P. M.; Jankowiak, A.; Gavilan, E.; Scheinost, A. C.; Herlet, N.; Dehaudt, P.; Blanchart, P. *Inorg. Chem.* **2011**, *50*, 12437−12445.
(18) Prieur, D.; Martin, P. M.; Lebreton, F.; Delahaye, T.; Jankowiak, A.; Laval, J.-P.; Scheinost, A. C.; Dehaudt, P.; Blanchart, P. *J. Solid State Chem.* **2012**, *194*, 206−211.
(19) Prieur, D.; Martin, P.; Lebreton, F.; Delahaye, T.; Banerjee, D.; Scheinost, A. C.; Jankowiak, A. *J. Nucl. Mater.* **2013**, *434*, 7−16.
(20) Lebreton, F.; Martin, P. M.; Horlait, D.; Bès, R.; Scheinost, A. C.; Rossberg, A.; Delahaye, T.; Blanchart, P. *Inorg. Chem.* **2014**, *53*, 9531−9540.
(21) Caisso, M.; Picart, S.; Belin, R. C.; Lebreton, F.; Martin, P. M.; Dardenne, K.; Rothe, J.; Neuville, D. R.; Delahaye, T.; Ayral, A. *Dalton Trans.* **2015**, *44*, 6391−6399.
(22) Prieur, D.; Lebreton, F.; Martin, P.; Caisso, M.; Butzbach, R.; Scheinost, A. C.; Somers, J.; Delahaye, T. *J. Solid State Chem.* **2015**, *230*, 8−13.
(23) Horlait, D.; Lebreton, F.; Roussel, P.; Delahaye, T. *Inorg. Chem.* **2013**, *52*, 14196−14204.
(24) Shannon, R. D. *Acta Crystallogr., Sect. A: Cryst. Phys., Diffr., Theor. Gen. Crystallogr.* **1976**, *32*, 751−767.
(25) Bartscher, W.; Sari, C. *J. Nucl. Mater.* **1983**, *118*, 220−223.
(26) Lebreton, F.; Horlait, D.; Delahaye, T.; Blanchart, P. *J. Nucl. Mater.* **2013**, *439*, 99−102.
(27) Mayer, K.; Kanellakopoulos, B.; Naegele, J.; Koch, L. *J. Alloys Compd.* **1994**, *213-214*, 456−459.
(28) Suzuki, C.; Nishi, T.; Nakada, M.; Tsuru, T.; Akabori, M.; Hirata, M.; Kaji, Y. *J. Phys. Chem. Solids* **2013**, *74*, 1769−1774.
(29) Prieur, D.; Lebreton, F.; Martin, P. M.; Jankowiak, A.; Delahaye, T.; Dehaudt, P.; Blanchart, P. *J. Eur. Ceram. Soc.* **2012**, *32*, 1585−1591.
(30) Lebreton, F.; Belin, R. C.; Prieur, D.; Delahaye, T.; Blanchart, P. *Inorg. Chem.* **2012**, *51*, 9369−9375.
(31) Horlait, D.; Feledziak, A.; Lebreton, F.; Clavier, N.; Prieur, D.; Dacheux, N.; Delahaye, T. *J. Nucl. Mater.* **2013**, *441*, 40−46.
(32) Rodríguez-Carvajal, J. *Phys. B* **1993**, *192*, 55−69.
(33) Le Bail, A. *Powder Diffr.* **2005**, *20*, 316−326.
(34) Thompson, P.; Cox, D. E.; Hastings, J. B. *J. Appl. Crystallogr.* **1987**, *20*, 79−83.
(35) Leinders, G.; Cardinaels, T.; Binnemans, K.; Verwerft, M. *J. Nucl. Mater.* **2015**, *459*, 135−142.
(36) Newville, M. *J. Synchrotron Radiat.* **2001**, *8*, 322−324.
(37) Ravel, B.; Newville, M. *J. Synchrotron Radiat.* **2005**, *12*, 537−541.
(38) Kvashnina, K. O.; Butorin, S. M.; Martin, P.; Glatzel, P. *Phys. Rev. Lett.* **2013**, *111*, 253002.
(39) Arab-Chapelet, B.; Grandjean, S.; Nowogrocki, G.; Abraham, F. *J. Alloys Compd.* **2007**, *444−445*, 387−390.
(40) Arab-Chapelet, B.; Grandjean, S.; Nowogrocki, G.; Abraham, F. *J. Nucl. Mater.* **2008**, *373*, 259−268.
(41) Arab-Chapelet, B.; Grandjean, S.; Costenoble, S.; Delahaye, T.; Martin, P.; Abraham, F. *Inorg. Chem.* **2015**.
(42) Jégou, C.; Caraballo, R.; Peuget, S.; Roudil, D.; Desgranges, L.; Magnin, M. *J. Nucl. Mater.* **2010**, *405*, 235−243.
(43) Caraballo, R.; Jégou, C.; Peuget, S.; Magnin, M. *HOTLAB 2013*, Idaho Falls, ID, 2013.
(44) Horlait, D.; Caraballo, R.; Lebreton, F.; Jégou, C.; Roussel, P.; Delahaye, T. *J. Solid State Chem.* **2014**, *217*, 159−168.
(45) Jegou, C.; Gennisson, M.; Peuget, S.; Desgranges, L.; Guimbretière, G.; Magnin, M.; Talip, Z.; Simon, P. *J. Nucl. Mater.* **2015**, *458*, 343−349.
(46) Naji, M.; Colle, J.-Y.; Beneš, O.; Sierig, M.; Rautio, J.; Lajarge, P.; Manara, D. *J. Raman Spectrosc.* **2015**, DOI: 10.1002/jrs.4716.
(47) Prieur, D.; Pagliosa, G.; Spino, J.; Caciuffo, R.; Somers, J.; Eloirdi, R. *J. Solid State Chem.* **2013**, *199*, 334−337.
(48) Chikalla, T. D.; Eyring, L. *J. Inorg. Nucl. Chem.* **1968**, *30*, 133−145.
(49) Hurtgen, C.; Fuger, J. *Inorg. Nucl. Chem. Lett.* **1977**, *13*, 179−188.
(50) Lebreton, F.; Belin, R. C.; Delahaye, T.; Blanchart, P. *J. Solid State Chem.* **2012**, *196*, 217−224.
(51) Weber, W. H.; Hass, K. C.; McBride, J. R. *Phys. Rev. B: Condens. Matter Mater. Phys.* **1993**, *48*, 178−185.
(52) Keramidas, V. G.; White, W. B. *J. Am. Ceram. Soc.* **1974**, *57*, 22−24.
(53) Sarsfield, M. J.; Taylor, R. J.; Puxley, C.; Steele, H. M. *J. Nucl. Mater.* **2012**, *427*, 333−342.
(54) Begun, G. M.; Haire, R. G.; Wilmarth, W. R.; Peterson, J. R. *J. Less-Common Met.* **1990**, *162*, 129−133.
(55) Manara, D.; Renker, B. *J. Nucl. Mater.* **2003**, *321*, 233−237.
(56) Livneh, T.; Sterer, E. *Phys. Rev. B: Condens. Matter Mater. Phys.* **2006**, *73*, 085118.
(57) He, H.; Shoesmith, D. *Phys. Chem. Chem. Phys.* **2010**, *12*, 8108−8118.
(58) Horlait, D.; Clavier, N.; Dacheux, N.; Cavalier, R.; Podor, R. *Mater. Res. Bull.* **2012**, *47*, 4017−4025.
(59) Desgranges, L.; Baldinozzi, G.; Simon, P.; Guimbretière, G.; Canizares, A. *J. Raman Spectrosc.* **2012**, *43*, 455−458.
(60) McBride, J. R.; Hass, K. C.; Poindexter, B. D.; Weber, W. H. *J. Appl. Phys.* **1994**, *76*, 2435−2441.
(61) Nakajima, A.; Yoshihara, A.; Ishigame, M. *Phys. Rev. B: Condens. Matter Mater. Phys.* **1994**, *50*, 13297−13307.
(62) Horlait, D.; Claparède, L.; Clavier, N.; Szenknect, S.; Dacheux, N.; Ravaux, J.; Podor, R. *Inorg. Chem.* **2011**, *50*, 7150−7161.
(63) Desgranges, L.; Pontillon, Y.; Matheron, P.; Marcet, M.; Simon, P.; Guimbretière, G.; Porcher, F. *Inorg. Chem.* **2012**, *51*, 9147−9149.
(64) Talip, Z.; Wiss, T.; Raison, P. E.; Paillier, J.; Manara, D.; Somers, J.; Konings, R. J. M. *J. Am. Ceram. Soc.* **2015**, *98*, 2278−2285.

DOI: 10.1021/acs.inorgchem.5b01357
Inorg. Chem. 2015, 54, 9749−9760

(65) Ravindran, T. R.; Krishnan, R. V. *Vib. Spectrosc.* **2014**, *73*, 97−101.
(66) Rao, R.; Bhagat, R. K.; Salke, N. P.; Kumar, A. *Appl. Spectrosc.* **2014**, *68*, 44−48.
(67) Taniguchi, T.; Watanabe, T.; Sugiyama, N.; Subramani, A. K.; Wagata, H.; Matsushita, N.; Yoshimura, M. *J. Phys. Chem. C* **2009**, *113*, 19789−19793.
(68) Guimbretière, G.; Desgranges, L.; Canizarès, A.; Carlot, G.; Caraballo, R.; Jégou, C.; Duval, F.; Raimboux, N.; Ammar, M. R.; Simon, P. *Appl. Phys. Lett.* **2012**, *100*, 251914.
(69) Razdan, M.; Shoesmith, D. W. *J. Electrochem. Soc.* **2014**, *161*, H105−H113.
(70) Prieur, D.; Jankowiak, A.; Roudil, D.; Dubois, S.; Leorier, C.; Herlet, N.; Dehaudt, P.; Laval, J.-P.; Blanchart, P. *J. Nucl. Mater.* **2011**, *411*, 15−19.
(71) Nishi, T.; Nakada, M.; Suzuki, C.; Shibata, H.; Okamoto, Y.; Akabori, M.; Hirata, M. *J. Nucl. Mater.* **2011**, *418*, 311−312.
(72) He, H.; Broczkowski, M.; O'Neil, K.; Ofori, D.; Semenikhin, O.; Shoesmith, D. *Corrosion of Nuclear Fuel (UO_2) Inside a Failed Nuclear Waste Container*; NWMO TR-2012-09;Western University: Ontario, Canada, 2012; p 67.
(73) Conradson, S. D.; Manara, D.; Wastin, F.; Clark, D. L.; Lander, G. H.; Morales, L. A.; Rebizant, J.; Rondinella, V. V. *Inorg. Chem.* **2004**, *43*, 6922−6935.
(74) Conradson, S. D.; Begg, B. D.; Clark, D. L.; den Auwer, C.; Ding, M.; Dorhout, P. K.; Espinosa-Faller, F. J.; Gordon, P. L.; Haire, R. G.; Hess, N. J.; Hess, R. F.; Webster Keogh, D.; Lander, G. H.; Manara, D.; Morales, L. A.; Neu, M. P.; Paviet-Hartmann, P.; Rebizant, J.; Rondinella, V. V.; Runde, W.; Drew Tait, C.; Kirk Veirs, D.; Villella, P. M.; Wastin, F. *J. Solid State Chem.* **2005**, *178*, 521−535.
(75) Conradson, S. D.; Durakiewicz, T.; Espinosa-Faller, F. J.; An, Y. Q.; Andersson, D. A.; Bishop, A. R.; Boland, K. S.; Bradley, J. A.; Byler, D. D.; Clark, D. L.; Conradson, D. R.; Conradson, L. L.; Costello, A. L.; Hess, N. J.; Lander, G. H.; Llobet, A.; Martucci, M. B.; Mustre de Leon, J.; Nordlund, D.; Lezama-Pacheco, J. S.; Proffen, T. E.; Rodriguez, G.; Schwarz, D. E.; Seidler, G. T.; Taylor, A. J.; Trugman, S. A.; Tyson, T. A.; Valdez, J. A. *Phys. Rev. B: Condens. Matter Mater. Phys.* **2013**, *88*, 115135.
(76) McEachern, R. J.; Taylor, P. *J. Nucl. Mater.* **1998**, *254*, 87−121.
(77) Wilson, W. B.; Alexander, C. A.; Gerds, A. F. *J. Inorg. Nucl. Chem.* **1961**, *20*, 242−251.
(78) Tennery, V. J.; Godfrey, T. G. *J. Am. Ceram. Soc.* **1973**, *56*, 129−133.
(79) Thomas, L. E.; Einziger, R. E.; Buchanan, H. C. *J. Nucl. Mater.* **1993**, *201*, 310−319.

DOI: 10.1021/acs.inorgchem.5b01357
Inorg. Chem. 2015, 54, 9749−9760